GA–A26240

INTRINSIC ROTATION
IN H-MODE PEDESTAL IN DIII-D

by
J.S. deGRASSIE, R.J. GROEBNER, K.H. BURRELL, and W.M. SOLOMON

SEPTEMBER 2008

GENERAL ATOMICS

DISCLAIMER

GA–A26240

INTRINSIC ROTATION
IN H-MODE PEDESTAL IN DIII-D

by
J.S. deGRASSIE, R.J. GROEBNER, K.H. BURRELL, and W.M. SOLOMON*

*Princeton Plasma Physics Laboratory, Princeton, New Jersey.

GENERAL ATOMICS PROJECT 30200
SEPTEMBER 2008

GENERAL ATOMICS

Intrinsic Rotation in H-mode Pedestal in DIII-D

J.S. deGrassie 1), R.J. Groebner 1), K.H. Burrell 1), and W.M. Solomon 2)

1) General Atomics, PO Box 85608, San Diego, California 92186-5608, USA
2) Princeton Plasma Physics Laboratory, Princeton, New Jersey 08543-0451, USA

e-mail contact of main author: degrassie@fusion.gat.com

Abstract. Intrinsic toroidal rotation in the tokamak exists with no auxiliary momentum input. Possible explanations are given by several theories, both from classical and turbulent considerations. A boundary condition for intrinsic rotation must be known to compute an absolute rotation profile with any theory. In DIII-D H-modes, we measure an intrinsic toroidal velocity in the pedestal that is in the co-I_p direction and is roughly proportional to the local ion temperature, T_i. A simple model of thermal ion orbit loss approximately demonstrates this T_i scaling, and predicts an inverse proportionality to the poloidal magnetic field strength. Experimentally, the T_i scaling of intrinsic velocity is also found inside the pedestal, where thermal ion orbit loss should be negligible. We postulate a momentum pinch in this region to produce this scaling inside the pedestal.

1. Introduction

Even with no auxiliary injected toroidal torque the plasma in a tokamak discharge is observed to have a nonzero toroidal flow velocity. We refer to this as "intrinsic rotation". A large variety of intrinsic rotation profiles have been measured [1–8]. One common result is that in diverted H-mode discharges the toroidal velocity, V_ϕ, increases in the direction of the plasma current, co-I_p, with increasing plasma stored energy [1,2]. Toroidal rotation is known to positively impact MHD stability [9] and energy confinement [10] and so it is important to be able to project present measurements to ITER, where neutral beam injected (NBI) torque will be relatively small.

A database of intrinsic rotation results from a number of the world's tokamaks indicates that in general $V_\phi \sim W/I_p$, where W is the plasma stored energy. An experimental effort is underway to probe this Rice scaling [7,8] further, and to determine if it can be cast in dimensionless parameters, increasing greatly the confidence level in extrapolation to ITER.

There are a number of theories that predict the existence of an intrinsic rotation, both in higher order neoclassical treatments [11–13], and in treatments of turbulence [14–21]. Turbulence can generate an internal source through a Reynolds stress effect, and both types of theory predict a radial momentum pinch, which may carry any boundary momentum, or source, inward. Without a source a pinch does nothing, so the boundary condition for intrinsic rotation becomes very important to understand. Additionally, any theory will need to include the boundary condition in order to predict an absolute rotation profile [17].

We find that the experimentally measured boundary condition for intrinsic rotation in DIII-D is consistent with a simple model of thermal ion orbit loss from the pedestal region. The experimental signature is that V_ϕ increases in the co-I_p direction roughly linearly with the local ion temperature, T_i. Our model for the loss cone in velocity space reproduces this scaling in the applicable regime in which only a small fraction of the counter-I_p thermal ions are lost to the divertor region (X-point). This is a collisionless treatment of the orbits, and thus an approximation, perhaps setting an upper bound for the effect. We note that a recent particle simulation of a DIII-D NBI-driven H-mode discharge that also includes collisions indicates that thermal ion orbit loss results in a co-I_p velocity just inside the last closed flux surface (LCFS) [22].

Classical, collisionless thermal ion orbit loss is an edge phenomenon. It has practical significance only in the pedestal region of the H-mode discharge, and thus, this mechanism may

be more important in the H-mode wherein the pedestal brings high density plasma near the LCFS, at minor radius $r=a$ on the outer midplane. The scaling of our loss-cone model is that the uncompensated co-I_p toroidal velocity in the pedestal region scales inversely with B_θ and linearly with T_i. This boundary condition then is effectively of diamagnetic form, $V_\phi(a) \sim T_i/B_\theta L$, where L is a parameter with the units of length. If this boundary condition is dominant, then the full profile of V_ϕ would be generally diamagnetic, in keeping with recent work by Waltz *et al.* [17].

Experimentally we further measure that $V_\phi \sim T_i$ inside of the pedestal region, beyond the range of guiding center loss of thermal ions. We hypothesize that in this region the boundary condition is carried inward by a momentum pinch mechanism that must be dependent upon the gradient in T_i, to have this scaling. Recent theories of the turbulent momentum pinch can exhibit this dependence.

2. Intrinsic Velocity in the Outer and Pedestal Regions in DIII-D

2.1 Pedestal Measurements

The DIII-D intrinsic rotation discharge database consists largely of H-modes created with ECH, and Ohmic heating (OH). There are some data also from time slices prior to the H-mode transition. The velocity profile results and the measurement techniques have been described previously [2,23]. Here we will focus upon the outer region in minor radius, $\rho>0.8$, and the pedestal region, $\rho>0.93$, where ρ is the normalized toroidal flux minor radius variable. The majority of our data is for measurements of T_i and velocity of the minor impurity constituent, C^{6+}, in bulk ion D^+ discharges. We also have a limited data set of bulk ion T_i and velocity measurements for He^{++} discharges [2,24,25]. To date we have observed nothing in the bulk ion intrinsic velocity measurements that would lead us to suspect that measurements of C^{6+} are misleading regarding scaling or general features of the results.

Figure 1 shows profiles measured in this spatial region in an ECH H-mode with negligible NBI torque impulse [23]. This is a lower single null (LSN) discharge with the
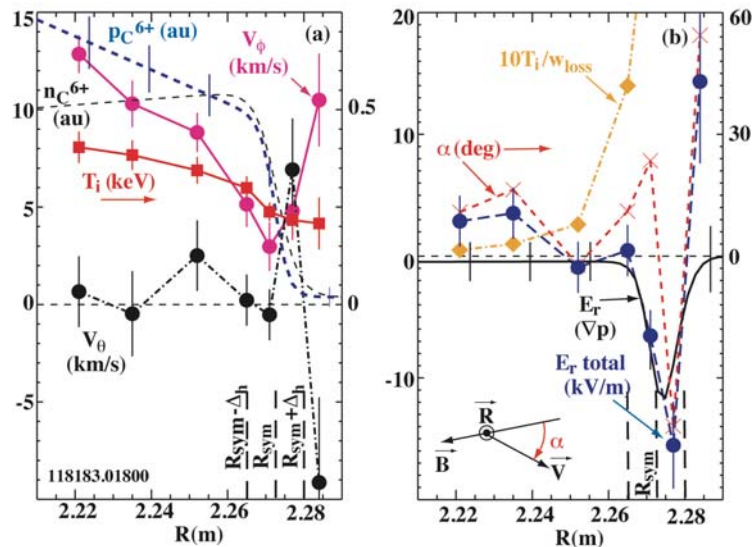

FIG. 1. ECH H-mode intrinsic velocity profiles on the outside midplane $\rho>0.8$. (a) Measured toroidal, V_ϕ (solid magenta), and poloidal V_θ (dot-dash black) ion velocity, T_i (red solid), and the Tanh-fits to the measured C^{6+} pressure, p_{C6+}, and density, n_{C6+} profiles (dash black). (b) Computed edge E_r, total (solid black) and ∇p (dash blue) term, angle, α (dash red), between V and B as indicated, T_i/W_{loss} (dot dash, gold, defined in Sec. 3). The middle vertical dashed line indicates R_{sym} for the n_{C6+} density fit, and the other two are separated from this by Δ_h.

$\vec{B} \times \vec{\nabla}B$ drift direction toward the X-point. Charge exchange recombination (CER) spectroscopy [26] is used to measure the edge radial profile of the C^{6+} relative density profile, and this is shown in Fig. 1(a) as $n_{C^{6+}}$. The CER measured T_i profile is shown and the two are used to construct the relative pressure profile, $p_{C^{6+}}$. The now-familiar pedestal tanh-fit [27] is used to specify the pedestal, and is described by the three vertical lines in Fig. 1. The central line is at the symmetry point (inflection of tanh), $R_{sym} = 2.273$ m, and the other two are separated from this by the half width, $\Delta_h = 7.5$ mm. The measurements of the V_ϕ and V_θ profiles are also shown in Fig. 1(a), with positive in the co-I_p direction, and the electron diamagnetic direction, respectively.

The radial electric field component computed from the gradient of the tanh-fit $p_{C^{6+}}$ profile, $E_r(\nabla p)$, is shown in Fig. 1(b) by the solid line, together with the total E_r using radial force balance. The computed pitch angle, α, between $\vec{V}$ and $\vec{B}$, as indicated, is plotted in degrees. Because of the magnitude of the error bars on $\vec{V}_\theta$, at only two locations is the value of α significant; just inside the top of the pedestal ($R = 2.252$ m) where $\vec{V}$ is antiparallel to $\vec{B}$ (i.e. V_ϕ is co-I_p), and near the foot of the pedestal ($R = 2.277$ m) where $\vec{V}_\theta$ makes a significant contribution to the negative electric field well.

The other computed quantity plotted in Fig. 1(b) is T_i/W_{loss}, scaled up x10 for convenience. W_{loss} is an energy parameter we will define that specifies ion orbit loss from the edge. Only if T_i/W_{loss} is non-negligible is thermal ion orbit loss active. This is the case just inside the top of the pedestal and further out.

The electron density profile, n_e, measured with Thomson scattering, also shows the pedestal structure in this region, as does the electron temperature, T_e. The gradient in T_i in the pedestal, as seen in Fig. 1(a), is much smaller than for any of these other kinetic profiles.

2.2 V_ϕ Scaling

In Fig. 2, we plot the measured V_ϕ vs T_i at the location just inside the top of the pedestal ($R = 2.251$), for 51 intrinsic rotation LSN discharges in the DIII-D database. We see a clear linear correlation in these data. The line drawn is from a simple straight line fit.

If NBI torque is added to these intrinsic rotation conditions, the pedestal region velocity is found to increase (co-I_p), or decrease (counter- I_p) depending upon the direction and details of the NBI torque profile applied, as shown by the small cross symbols in background. This is true for the channels extending to the bottom of the pedestal. That is, this boundary velocity is not fixed in these diverted discharges, but can be accelerated in either direction.

The CER channel locations in the multiple shot database are not all at exactly the same position relative to the pedestal as depicted in Fig. 1, due to small variations in the equilibria surface locations in different discharges. But this variation does not wash out the scaling of $V_\phi \sim T_i$ because this correlation holds through-

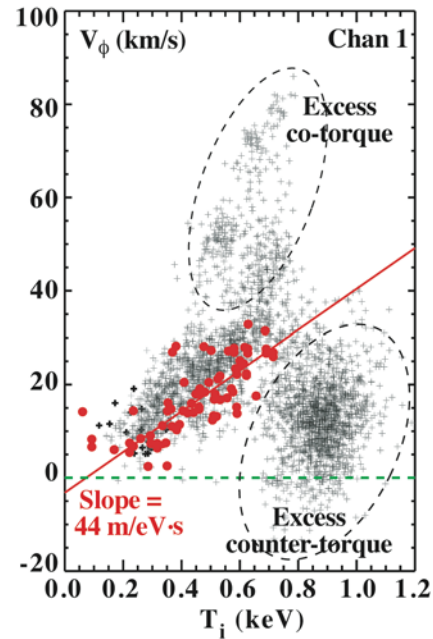FIG. 2. V_ϕ vs T_i for dataset of 51 discharges in intrinsic rotation conditions (red circles) for channel located in Fig. 1 at $R = 2.223$ m, just inside the top of the pedestal. The straight line is a simple fit. The other points are with added NBI torque: greater positive V_ϕ, greater negative, and little changed V_ϕ with the addition of co-, counter-, and near balanced NBI torque, respectively.

out the region ρ>0.8 with a similar proportionality constant. We show in Fig. 3 data from the inner 5 CER channels used in Fig. 1, all displayed on the same plot. Although there is more scatter in the correlation, it is still clear that $V_\phi \sim T_i$, although it might appear that a power slightly larger than linear would be appropriate for T_i.

The DIII-D intrinsic rotation database with bulk ion helium discharges also displays this correlation between V_ϕ and T_i. The database is too scant to allow a meaningful proportionality constant to be fit, but the indication is that the slope is ≈1/2 that of the carbon data in D^+ discharges.

3. Thermal Ion Orbit Loss Model

A number of authors have treated thermal ion orbit loss in poloidally diverted tokamak equilibria [22,28–31]. We assume that ions are only lost in the vicinity of the X-point, that no other limiting surface acts to interrupt a collisionless orbit outside the LCFS. The orbits most readily lost are those on the outboard midplane in the pedestal region with

FIG. 3. V_ϕ vs T_i for the DIII-D intrinsic rotation dataset using the five inner channels shown in Fig. 1. The line is a simple fit. The measured ion is C^{6+}.

parallel velocity counter to I_p [29]. These lost orbits leave a hole in velocity space in the pedestal region that results in a net average co-I_p parallel velocity in the distribution function left behind. Collisions repopulate the loss cone and also affect the orbits as they move toward the X-point, and must be considered for any ultimate quantitative comparison with experiment. Nevertheless, our simplified collisionless approximation serves to understand the origin, and possibly establish the scaling.

We assume that the pedestal region has come to steady state and thus whatever mechanism sets the pedestal negative electric field well has already done so. We neglect the effect of E_r on the loss orbit dynamics. For these intrinsic rotation discharges we find that $\rho_\theta E_r \ll T_i$, where ρ_θ is the poloidal ion gyroradius, and thus the potential well represents a correction to the loss cone [29], which can be considered in our treatment as a perturbation. Neglect of the potential well is not necessarily warranted for high power NBI H-modes in DIII-D.

In steady state there must be a return current to balance the outward ion orbit loss current. Usually an ion frictionally-driven return current is invoked, but it could be supplied by anomalous electron loss from the pedestal region. We assume that only the mechanical momentum of the lost ions need be considered, and hence the deficit in velocity space.

To define a thermal ion guiding center loss orbit we consider the starting location of a midplane orbit to be at $R = R_1$, on the surface $\psi = \psi_1$, where ψ is the poloidal flux function, which increases with ρ for usual DIII-D field directions. The starting location is inside the boundary surface, $\psi_1 < \psi_x$. Our criterion for a lost orbit is simply that $\psi > \psi_x$ when the orbit is at major radial location $R = R_x$ (i.e. vertical location in a LSN $Z < Z_x$). For standard DIII-D conditions, $I(\psi) < 0$ and $V_\phi = (B_\phi/B)V_\| \approx -V_\|$, where $V_\| \equiv V\cos(p)$ defines the pitch angle, p.

We use the three constants of the motion; magnetic moment, total energy, and canonical toroidal angular momentum to compute the loss boundaries in phase space in general. However, we find some simplifying approximations are useful, and valid in that they well-approximate full ion guiding center numerical orbit calculations. We assume $I = \sigma_\phi R_0 B_0$, a constant, where σ_ϕ is the sign of the toroidal field. We neglect $(B_\theta/B_\phi)^2$. With the further
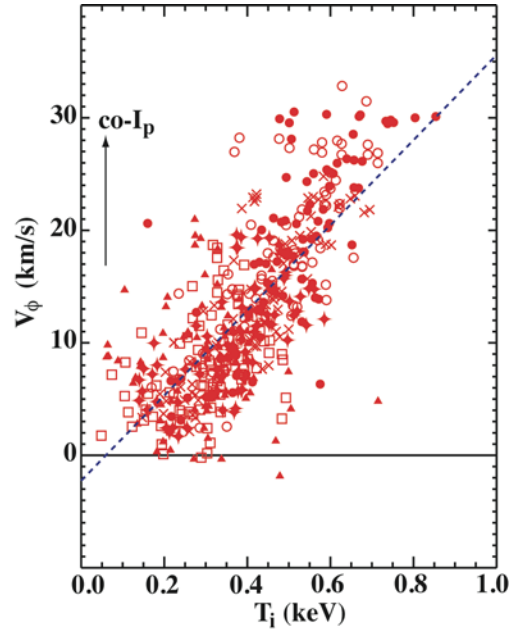
approximation that a barely trapped outboard starting ion turns on the same ψ_1 flux surface, the pitch angle of the trapped/passing boundary in velocity space is $p = p_t = \sin^{-1}(\sqrt{R_{1in}/R_1})$, and the pitch angle of a trapped ion with turning point at the $R = R_x$ surface is likewise $p = p_x = \sin^{-1}(\sqrt{R_x/R_1})$. Ions with starting pitch $p_1 > p_x$ do not reach the R_x surface and cannot be lost by our criterion. Here, the inboard location of the ψ_1 surface at $(R_{1in}, Z=0)$ defines R_{1in}.

With these approximations the loss cone boundary in the midplane edge region is defined by

$$\frac{1}{\sqrt{\alpha_E}} \leq -\sigma_\phi \cos(p_1) \pm \sigma_\phi (R_x/R_1)\sqrt{1-(R_1/R_x)\sin^2(p_1)} \quad, \tag{1}$$

where we have introduced $\alpha_E \equiv (MV_0^2/2)/W_{loss}$ with $W_{loss} \equiv M\Delta^2 \omega_\theta^2/2$, $\omega_\theta \equiv ZeB_{\theta 1}/M$, and V_0 is the starting velocity. We have expanded near the starting point with $\psi_x - \psi_1 \approx R_1 B_{\theta 1}\Delta$, where $\Delta = R_L - R_1$, the distance between these surfaces on the midplane. The parameter W_{loss} basically defines the energy necessary for an orbit to be lost, scaling as Z^2/M at a fixed starting location, and $\sqrt{\alpha_E} \sim \rho_\theta/\Delta$.

In Fig. 4 we show the loss region in (α_E, p_1) space, computed with Eq. (1), using the equilibrium shape of the LSN DIII-D discharge for the data in Fig. 1. The dominant region, with the finger-like structure, for outboard counter lost ions, all with $p_1 < \pi/2$, qualitatively reproduces that determined by Chankin and McCracken using numerical orbit computations [29]. The sign choice on the right side of Eq. (1) depends upon the direction of $V_\parallel$ when passing the X-point. The most readily lost ion, the smallest α_E, is a barely trapped ion that is coming back to the X-point from inboard with co-I_p $V_\parallel$ and sufficient kinetic energy to drift into ψ_x (red area in Fig. 4). In Fig. 4 we also show the region for co-I_p $V_\parallel$ ions to be lost from the inboard midplane edge for completeness. The absolute energy threshold for such an inboard co-I_p ion to be lost from the same surface is much greater than from the finger region. To compute the ion flow velocity, $\langle V_\parallel \rangle$, we assume that the distribution function is empty in the loss region indicated in Fig. 4. The remainder of the distribution function is taken to be a Maxwellian, f_M, with temperature T_i. That is, the distribution is $f = f_M(1-g)$, where $g=1$ in the loss region and 0 outside of it. The exponential dependence of $\exp(-\alpha_E W_{loss}/T_i)$ in the integration limit makes the outboard "finger" region dominant, so we only consider this region for loss. Further, to obtain an analytic result, we approximate this region by the area bounded by $p_x < p_1 < p_t$ and $\alpha_E \geq \alpha_E^{AV}$ where $\alpha_E^{AV} \equiv \alpha_E(\bar{p})$ on the loss boundary, with $\bar{p} = (p_t + p_x)/2$. This approximation makes less than a 10% difference compared with a full numerical integration.

Our result can be written $\langle V_\parallel \rangle \approx -(2/\pi)^{1/2}\bar{V}(b+1)e^{-b}(x-r_1)/2D(b,x,r_1)$, where the denominator term, D, here makes less than a 10% correction. The minus sign means that this flow velocity is in the co-I_p direction in these DIII-D conditions. Here, $\bar{V} = 2\sqrt{T_i/M}$, $r_1 = R_{1in}/R_1$, $b = \alpha_E^{av}(W_{loss}/T_i)$, $x = R_x/R_1$, $\alpha_E^{av} = \left[1/\sqrt{1-(x+r_1)/2} + x\sqrt{(1-r_1/x)/2}\right]^2$.
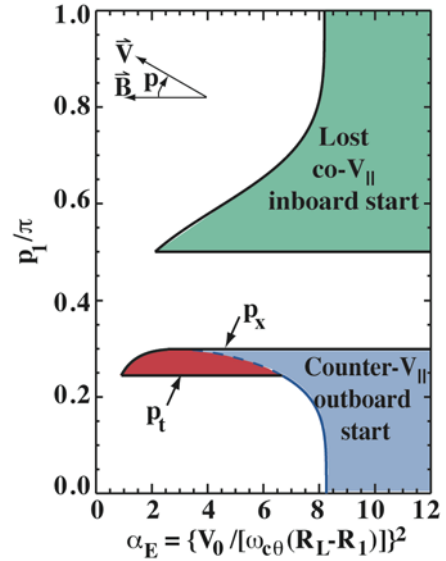

FIG. 4. Computed velocity space loss cone with starting pitch angle, p_1, vs α_E. Orbits with $p_1 < \pi/2$ have counter-I_p $V_\parallel$. The trapped/passing boundary is at $p_1 = p_t$, and at $p_1 = p_x$ an outboard starting ion will have a turning point at the $R = R_x$ surface.

The "diamagnetic" scaling with T_i/B_θ is evident if we plot this result with scaled variables, $-\langle V_\| \rangle / \sqrt{W_{loss}/M}$ vs T_i/W_{loss} and obtain approximate linearity, as shown in Fig. 5(a). The approximate linearity with T_i results from one power of $T_i^{1/2}$ due to $\bar{V}$, and roughly one more $T_i^{1/2}$ due to the variation with b. In order to obtain an absolute value for $-\langle V_\| \rangle \approx \langle V_\phi \rangle$, we must know Δ, the distance between the starting surface, i.e. the measurement location which is well known, and the LCFS. The accuracy in locating the LCFS with EFIT has been determined to be $\sim \pm 5$ mm from edge studies [32,33]. The sensitivity of $\langle V_\| \rangle$ is significant within this accuracy. In Fig. 5(b) we plot $-\langle V_\| \rangle$ vs T_i using three values of R_L, with the starting location at the measurement channel at the top of the pedestal shown in Fig. 1. The middle curve uses the EFIT-determined value, $R_L = R_{L0}$, with $\Delta = 18$ mm, and the other two have $R_L = R_{L0} \pm 5$ mm. The vertical and horizontal lines are at the measured values of T_i and V_ϕ, which falls well within the range of the error in boundary location.
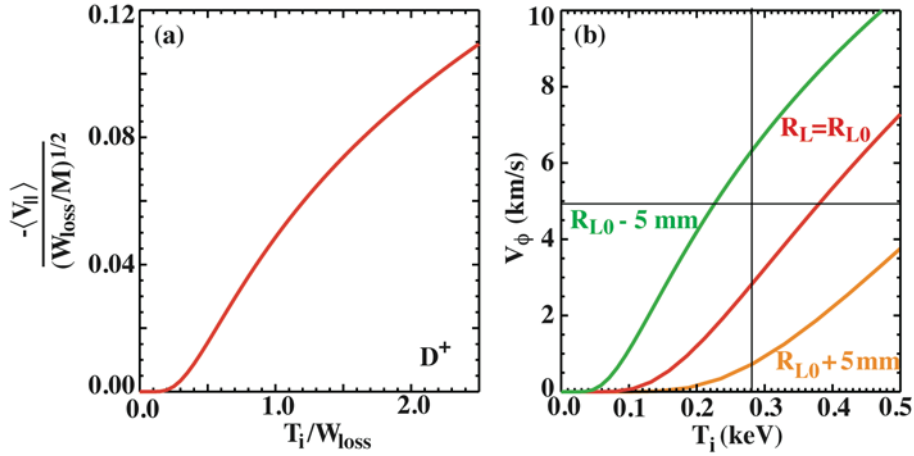

FIG. 5. (a) Scaled distribution-averaged co-I_p velocity, $\langle -V_\| \rangle$, computed with Eq. (3), vs T_i/W_{loss}, using the equilibrium conditions from discharge time in Fig. 1. (b) The middle line uses the result shown in (a) and computes an absolute value for V_ϕ for the channel at $R = 2.260$ m, at the top of the H-mode pedestal in Fig. 1. The two other lines use different locations of the LCFS, 5 mm closer to the measurement channel (green online), and 5 mm further away.

Detailed comparison of the orbit loss model with experiment will require a more accurate determination of the location of the LCFS, the projection of the X-point surface to the midplane. However, it is hoped that scaling for the pedestal boundary condition on intrinsic velocity can be further explored apart from this.

4. Momentum Pinch Phenomenology

Experimentally, the result $V_\phi \sim T_i$ continues well inside the top of the pedestal where classical, collisionless thermal ion orbit loss is not effective. From the plot of T_i/W_{loss} in Fig. 1(a) we see that our orbit loss model predicts a very small V_ϕ for the inner two channels. We conclude that some process is carrying the boundary scaling inward. We hypothesize that this may be due to the momentum pinch effect seen experimentally [34–37] and discussed theoretically [11–21].

A simple phenomenological case can be made that if the momentum pinch velocity, V^P, is driven by an ion temperature gradient term, $V^P \sim \partial T_i / \partial r$, the scaling of V_ϕ with T_i could ensue. Here we use r as a generic minor radius coordinate. There are qualitative theoretical predictions for such a turbulence-driven momentum pinch [15,16,18].

Consider the local toroidal flux surface averaged ($\langle * \rangle$) momentum density of the plasma, $\ell = M n_i \langle R^2 \rangle \omega_\phi$, where $V_\phi = R \omega_\phi$, and ω_ϕ is taken to be a function of ψ. Without an internal torque the radial flux of toroidal momentum at a surface must vanish, $-\chi_\phi(\partial \ell / \partial r) + V^P \ell = 0$, where χ_ϕ is the momentum diffusivity. Inside the pedestal in these H-mode intrinsic rotation discharges the density profile becomes quite flat relative to the T_i and V_ϕ profiles. By neglecting the density gradient we can replace ℓ in the zero momentum flux expression with V_ϕ, and rewrite it as $(\partial V_\phi / \partial r) / V_\phi = V^P / \chi_\phi$. The approximate proportionality of V_ϕ to T_i would result in this inside region if $V^P / \chi_\phi = k(\partial T_i / \partial r) / T_i$, with k near unity, so the solution for V_ϕ becomes $V_\phi = V_\phi(a) [T_i / T_i(a)]^k$, with the boundary condition specified at $r=a$. The data in Fig. 3 clearly leave room for k to be not exactly unity, but not too different. It may also be a weak function of r in this region.

Recent extensions to neoclassical theory predict an intrinsic toroidal rotation driven by a gradient in T_i [11–13]. However, the theoretical result in the collisional regime is that the square of the T_i gradient matters and the sign is such that a counter-I_p V_ϕ results. The collisionless result is not clear.

There are now a number of theoretical quasilinear treatments of toroidal momentum transport driven by turbulence that predict an intrinsic rotation [14–21]. These are set in slab, cylindrical, and toroidal geometry. In toroidal geometry Shaing's analytic treatment of the drift kinetic equations results in a pinch as we postulate if the density gradient is small [15]. Also, in a recent general treatment of drift wave turbulence and parallel momentum transport in cylindrical geometry, including considerations of turbulent wave momentum, Diamond *et al*. [18] also arrive at such an equation for the pinch for small density gradient.

5. Summary

In the pedestal region of intrinsic rotation H-mode discharges in DIII-D we measure a co-I_p toroidal velocity that is roughly linearly proportional to the local ion temperature. This scaling, and the magnitude of the velocity can be explained by a simple model for thermal ion orbit loss to the X-point region that leaves a counter-I_p hole in velocity space. This is a collisionless model, but in a recent pedestal simulation with collisions Chang and Ku [22] have invoked thermal ion orbit loss to create a co-I_p $V_\parallel$ just inside the LCFS. The approximate scaling $V_\phi \sim T_i$ results from our model. This boundary condition on intrinsic velocity in the pedestal region of an H-mode discharge will scale as

$$\vec{V}_\phi \sim (T_i / |B_\theta| L) \hat{I}_p \quad , \tag{2}$$

where L is some length, and $\hat{I}_p$ indicates the direction of the plasma current. To make a quantitative comparison with experiment is challenging due to the high accuracy required to locate the LCFS.

Although our measurements are for C^{6+}, the classical orbit loss of thermal C^{6+} from the pedestal is essentially nonexistent compared with D^+. The energy loss parameter, W_{loss}, scales as Z^2/M, so the parameter b for C^{6+} is much larger at the same T_i. We must assume that D^+, the bulk ion, is lost, creating the velocity space hole, and that C^{6+} is frictionally dragged along to acquire a velocity similar to that of D^+.

The scaling $V_\phi \sim T_i$ is also measured somewhat inside the pedestal, where orbit loss is not effective. We postulate a momentum pinch effect having $V^P \sim \nabla T_i$ to provide a phenomenological model for this scaling. Some recent theories of the turbulent momentum pinch find a similar result. Future experiments will explore the efficacy of this explanation.

Acknowledgments

References

[1]   RICE, J.E., *et al.*, Nucl. Fusion **47**, 1618 (2007), and references therein.
[2]   deGRASSIE, J.S., *et al.*, Phys. Plasmas **14**, 056115-1 (2007), and references therein.
[3]   ERIKSSON, L.-G., *et al.*, Plasma Phys. Control. Fusion **39**, 27 (1997).
[4]   ERIKSSON, L.-G., *et al.*, Nucl. Fusion **41**, 91 (2001).
[5]   DUVAL, B.P., *et al.*, Plasma Phys. Controlled Fusion **49**, B195 (2001).
[6]   YOSHIDA, M., *et al.*, Phys. Rev. Lett. **100**, 105002-1 (2008).
[7]   RICE, J.E., *et al.*, Nucl. Fusion **41**, 277 (2001).
[8]   HUTCHINSON, I.H., *et al.*, Phys. Rev. Lett. **84**, 3330 (2000).
[9]   STRAIT, E.J., *et al.*, Phys. Plasmas **14**, 056101 (2007).
[10]   POLITZER, P.A., *et al.*, Nucl. Fusion **48**, 075001 (2008).
[11]   WONG, S.K. and CHAN, V.S., Phys. Plasmas **14**, 112505 (2007).
[12]   CATTO, P.J. and SIMIKOV, A.N., Phys. Plasmas **12**, 012501 (2005).
[13]   CLAASSEN, H.A., *et al.*, Phys. Plasmas **7**, 3699 (2000).
[14]   DOMINGUEZ, R.R. and STAEBLER, G.M., Phys. Fluids B **5**, 3876 (1993).
[15]   SHAING, K.C., Phys. Plasmas **8**, 193 (2001).
[16]   COPPI, B., Nucl. Fusion **42**, 1 (2002).
[17]   WALTZ, R.E., *et al.*, Phys. Plasmas **14**, 122507 (2007).
[18]   DIAMOND, P.H., *et al.*, Phys. Plasmas **15**, 012303 (2008).
[19]   GURCAN, O.D., *et al.*, Phys. Rev. Lett. **100**, 135001 (2007).
[20]   HAHM, T.S., *et al.*, Phys. Plasmas **14**, 072302 (2007).
[21]   PEETERS, A.G., *et al.*, Phys. Rev. Lett. **98**, 265003-1 (2007).
[22]   CHANG, C.S and KU, S., Phys. Plasmas **15**, 62510 (2008).
[23]   deGRASSIE, J.S., *et al.*, Phys. Plasmas **11**, 4323 (2004).
[24]   deGRASSIE, J.S., *et al.*, Proc. of 20th Int. Conf. on Plasma Phys. and Control. Nucl. Fusion Research, 2004, Vilamoura, Portugal (IAEA, Vienna, 2005) Paper IAEA-CN-116-EX/604Rb.
[25]   deGRASSIE, J.S., *et al.*, Phys. Plasmas **13**, 112507 (2006).
[26]   BURRELL, K.H., *et al.*, Rev. Sci. Instrum. **72**, 1028 (2001).
[27]   GROEBNER, R.J., *et al.*, Fusion Sci. Technol. **48**, 1011 (2005).
[28]   KU, S., *et al.*, Phys. Plasmas **11**, 5626 (2004).
[29]   CHANKIN, A.V. and McCRACKEN, G.M., Nucl. Fusion **10**, 1459 (1993).
[30]   MIYAMOTO, K., Nucl. Fusion **36**, 927 (1996).
[31]   HEIKKINEN, J.A., *et al.*, Phys. Rev. Lett. **84**, 487 (2000).
[32]   LAO, L.L., *et al.*, Fusion Sci. Technol. **48**, 968 (2005).
[33]   PORTER, G.D., *et al.*, Phys. Plasmas **5**, 1410 (1998).
[34]   NAGASHIMA, M., *et al.*, Nucl. Fusion **34**, 449 (1994).
[35]   TALA, T., *et al.*, Plasma Phys. Control. Fusion **49**, B291 (2007).
[36]   YOSHIDA, M., *et al.*, Nucl. Fusion **47**, 856 (2007).
[37]   LEE, W.D., *et al.*, Phys. Rev. Lett. **91**, 205003-1 (2003).